NUMERICAL SIMULATION OF AIR NATURAL CIRCULATION AND THERMAL RADIATION IN PASSIVE CONTAINMENT COOLING SYSTEM

Weizhong Zhang and Qian Lin
Advanced Nuclear Power Technology R&D Center,
Shanghai Nuclear Engineering Research and Design Institute,
29 Hongcao Road, Xuhui, Shanghai 200233, China
zhangweizhong@snerdi.com.cn; linqian@snerdi.com.cn

ABSTRACT

Passive containment cooling system (PCS) is one of the most important passive safety systems in an AP1000 nuclear power plant. Numerical simulation of air natural circulation and thermal radiation in PCS without falling film was conducted using numerical method to investigate the air coolability of PCS. The results indicate that just with air natural circulation and thermal radiation, PCS can't remove all the core decay heat to the environment. The effects of geometrical size, steel containment vessel outside surface temperature and the environmental temperature on the air coolability were also investigated. With the increase of air inlet temperature, the heat transfer rate of thermal radiation and that of natural circulation decrease linearly. Air inlet temperature affects the heat transfer performance of natural circulation significantly, but it affects that of thermal radiation very little. With the increasing of steel containment vessel outside surface temperature, the natural circulation heat transfer rate increases almost linearly, how ever, the thermal radiation heat transfer rate tends to increase with a little bit faster pace. Geometry size affects the heat transfer rate of natural circulation significantly.

KEYWORDS
Natural circulation; Thermal radiation; Surface-to-surface model.

1. INTRODUCTION

The AP1000 is a nuclear power plant designed by Westinghouse Electric Company in accordance with the concept of passive nuclear safety. It introduced many passive safety systems, which greatly improves the safety of nuclear power plant [1]. Passive Containment cooling System (PCS) is one of them and removes heat from the containment during design basis events. The heat transfer mechanism of PCS inside and outside the containment was schematically shown in Fig. 1, and includes convection, heat conduction, thermal radiation and mass transfer (including internal condensation and external evaporation). PCS consists of several components to effectively cool the containment in the unlikely event of an accident so the design pressure is not exceeded, and the pressure is rapidly reduced. Natural circulation and water evaporation outside the steel containment vessel (CV) contribute to cooling the system. During a station blackout, or loss of all electrical power, the AP1000 plant's passive safety system shuts down the reactor automatically, with no need for human intervention for up to 72 hours. After 72 hours, if still without human intervention, there is no water resource in passive containment cooling water storage tank (PCCWST) located at the top of shielding building, and then there is no falling film and evaporation on the outside surface of the steel CV. The steel CV is only cooled by natural circulation of air and thermal radiation inside the annulus of the shielding building.

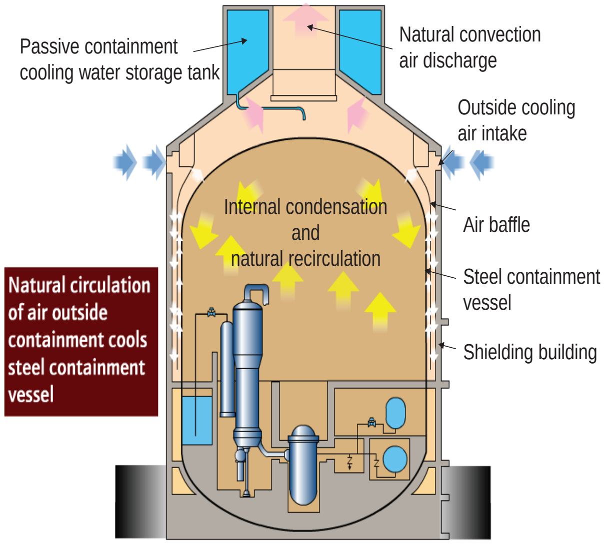

Figure 1. Schematic diagram of AP1000 PCS

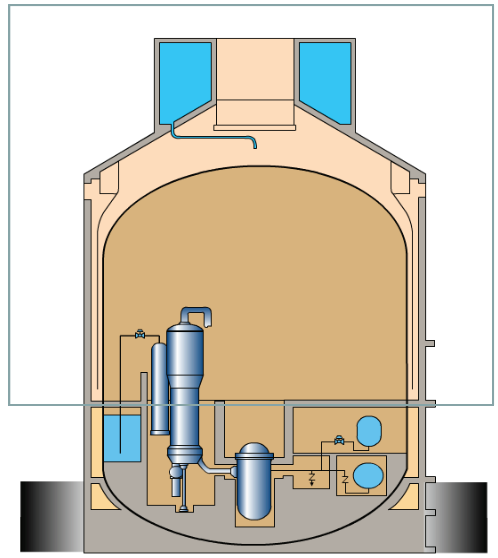

Figure 2. Upper part of AP1000 CV

Wang et al. [2] investigated the heat transfer performance of air natural circulation and thermal radiation in the annulus of the shielding building of the AP1000 by using CFD software ANSYS CFX. Their results indicated that at the time of 72 hours after break accident, the PCS can't completely remove reactor core decay heat to the environment just with the natural circulation and thermal radiation. They pointed out that the PCS heat removal power increases with the increase of the outside surface temperature of steel containment, and the fraction of thermal radiation in the PCS heat removal power is the smallest when the outside surface temperature of steel containment is 80 ^{o}C. This tendency is questionable and their explanation seems not sound. They didn't show the power tendency of natural circulation and that of thermal radiation separately. In their work, "Discrete Transfer Model" is used for thermal radiation.

In this paper, a similar numerical simulation of PCS without falling film by using ANSYS FLUENT ver. 14.0 [3] instead of CFX [2] was performed to investigate the heat transfer performance of air natural circulation and thermal radiation in the annulus of the shielding building. "Surface-to-Surface (S2S)

Figure 3. Whole View of PCS Model **Figure 4. Half View of PCS Model**

Model" was adopted for thermal radiation. The effects of inlet air temperature, steel CV outside surface temperature and geometrical size on the heat removal power of PCS will be reported.

2. GEOMETRY

The upper part of the containment of AP1000, denoted by a rectangle in Fig. 2, can be modeled as in Figures 3 and 4. This is an axis symmetric structure. In order to save computer resources, 30^o (1/12 of the PCS) sector is used in this paper, as shown in Fig. 5. The geometry includes the annulus space between the outside surface of steel CV and the inside surface of shielding building, the air baffle locating in the annulus is also included in the model. Other geometrical features such as the structures in the chimney space are omitted for simplification. Moreover, the increase of residence due to these structures is small because of large space in the upper part of the chimney. The total height of the geometry is about 40 m.

3. MATHEMATICAL MODEL

The temperature of outside surface of steel CV is much higher than the environmental temperature, which may induce a turbulent flow in the annulus of PCS. Whether the flow is turbulent or not will be checked later based only on Reynolds number, since the flow is natural circulation, instead of natural convection. Predictions using several different turbulence models and near-wall treatments were extensively evaluated and compared by Frisani et al. [4] to test the effect of turbulence modeling on the reactor cavity cooling system heat exchange. They reported that the k-ε turbulence models showed in general better performance than the k-ω and Spalart-Allmaras models if compared with the Reynolds Stress Transport results and experimental data. The standard k-ε turbulence model is used in the work of Wang et al [2]. It is also used in this simulation. Governing equations [2] are,

The continuity equation

$$\frac{\partial\rho}{\partial t} + \nabla(\rho u) = S_m \quad (1)$$

The momentum equation

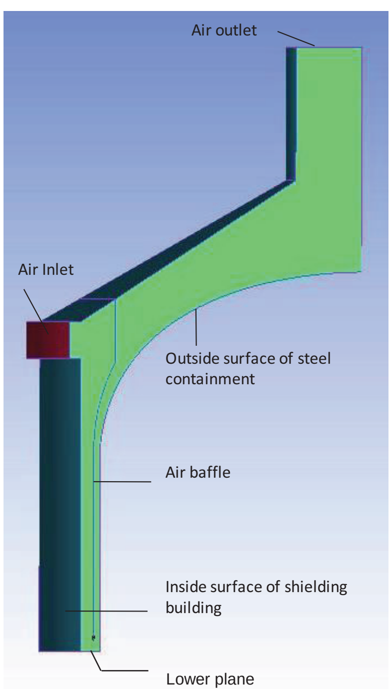

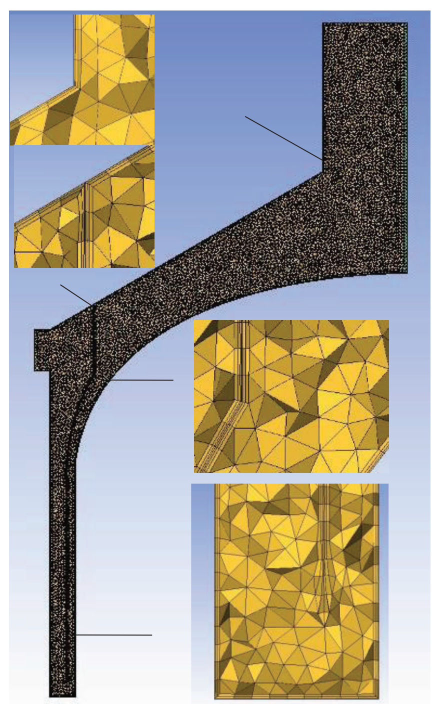

Figure 5. Computational Region **Figure 6. Mesh**

$$\rho\left(\frac{\partial u}{\partial t}+u\cdot\nabla u\right)=\rho f+\nabla\cdot\sigma \tag{2}$$

The energy equation

$$\rho C_p\left(\frac{\partial T}{\partial t}+u\cdot\nabla T\right)+\mathrm{p}\nabla u=(\nabla\lambda\cdot\nabla)T+\rho q-\nabla q_r+\phi \tag{3}$$

The k equation

$$\frac{\partial(\rho k)}{\partial t}+\frac{\partial(\rho \mathrm{k u_i})}{\partial \mathrm{x_i}}=\frac{\partial}{\partial \mathrm{x}}\left[\left(\mu+\frac{\mu_t}{\sigma_k}\right)\frac{\partial\varepsilon}{\partial \mathrm{x_j}}\right]+G_k+G_b-\rho\varepsilon-Y_M+S_k \tag{4}$$

The ε equation

$$\frac{\partial(\rho\varepsilon)}{\partial t}+\frac{\partial(\rho\varepsilon u_i)}{\partial x_i}=\frac{\partial}{\partial x}\left[\left(\mu+\frac{\mu_t}{\sigma_\varepsilon}\right)\frac{\partial\varepsilon}{\partial x_j}\right]+C_{1\varepsilon}\frac{\varepsilon}{k}(G_k+C_{3\varepsilon}G_b)-C_{2\varepsilon}\rho\frac{\varepsilon^2}{k}+S_\varepsilon \tag{5}$$

Where G_k and G_b are the rates of energy production due to shear and buoyancy; σ_k, σ_ε, $C_{1\varepsilon}$, $C_{2\varepsilon}$ and $C_{3\varepsilon}$ are empirical constants; Y_M is the contribution of pulsate expansion in compressible turbulence; u is fluid velocity.

In the simulation, the “Standard Wall Functions” option is selected for “Near-Wall Treatment”. The turbulent model constants are set to the defaults in the code [3], that is, C_μ to 0.09, $C_{1\varepsilon}$ to 1.44 and $C_{2\varepsilon}$ to 1.92.

In the problem discussed here, the air density in the annulus is not uniform due to temperature difference and then the natural circulation is induced. For the solution of natural circulation, the treatment of density is a key point. Following the way of Wang et al. [2], we also used the ideal gas model rather than the Boussinesq density model to do simulation due to big density difference in the annulus.

For thermal radiation calculation, it may be better to select a model based on a series of fundamental experiment analyses to show its validity and applicability. However, for comparison with the work by Wang et al. [2], we used a different thermal radiation model called “Surface-to-Surface (S2S) Model”, which assumes that any absorption, emission, or scattering of radiation by the medium can be ignored, and therefore only “surface-to-surface” radiation is considered for analysis. The S2S radiation model can be used to account for the radiation exchange in an enclosure of gray-diffuse surfaces. The energy exchange between two surfaces depends in part on their size, separation distance, and orientation. In this study, radiation heat transfer was calculated between any two of surfaces including the outside surface of steel CV, air baffle, inside surface of shielding building, and lower plane. The emissivity and diffuse fraction of each heat transfer surface are also set to 0.9 as in Wang et al. [2]. It should be mentioned that here the air baffle was taken as a surface, and thus has no thickness. In this way, it may accept heat from the outside surface of the steel CV, and transport it to the surrounding air by natural convection, to the inside surface of shielding building by radiation as well.

4. MESH AND BOUNDARY CONDITIONS

Computational mesh was auto-generated by ICEM CFD using the Delaunay approach. The volume mesh is tetra with 3 layers of prism near the wall, as shown in Fig. 6. The air baffle was modeled as a surface. To test grid independence, three different meshes were considered. Mesh convergence was reached with the total number of meshes and nodes being about 1.1 million and 257K respectively. The max element size is set to 0.2 m.

The design pressure and temperature of AP1000 steel CV were 0.50 MPa (abs) and 148.85 ºC, respectively. The PCS heat removal capability under the condition that the outside steel CV surface temperature is 148.85 ºC was calculated. If the heat removal power is larger than the core decay power, the pressure and temperature of inside containment will not rise, or else the core decay heat will threaten the integrity of containment. The air inlet and outlet were set as "pressure-inlet" and "pressure-outlet" conditions. The gauge total pressure at the air inlet was set to 235 Pascal, which took into account the air static pressure difference between the inlet and the outlet in the environment. Actually, the outlet pressure is not the atmosphere pressure due to the exiting buoyancy jet. Zero velocity gradients may be a better outlet condition to be considered. Then, in this case the inlet pressure can be set to the atmosphere pressure. In this paper, we choose the former inlet and outlet boundaries. Non-slip and adiabatic boundary conditions were applied at the inside surface of shielding building and the lower plane, and thus the temperatures of the surface and plane can be determined by calculation. We used just symmetries for the side borders. The outside surface temperature of the steel CV was assumed to be uniform. Due to thermal stratification inside the containment and varying local heat transfer rate, different temperature at different elevation should be the more reasonable assumption. Here for simplification we choose the former one. No conduction effects were considered in the present configuration. The gravitational acceleration was set to 9.81 m/s^2. "Body Force Weighted" was selected from the "Pressure" drop-down list in the "Spatial Discretization" group box [3]. Coupled scheme was selected for solving pressure-velocity coupling, and the second order upwind used for momentum and energy equations. The convergence criterion was set to 10^{-5}.

5. RESULTS AND DISCUSSION

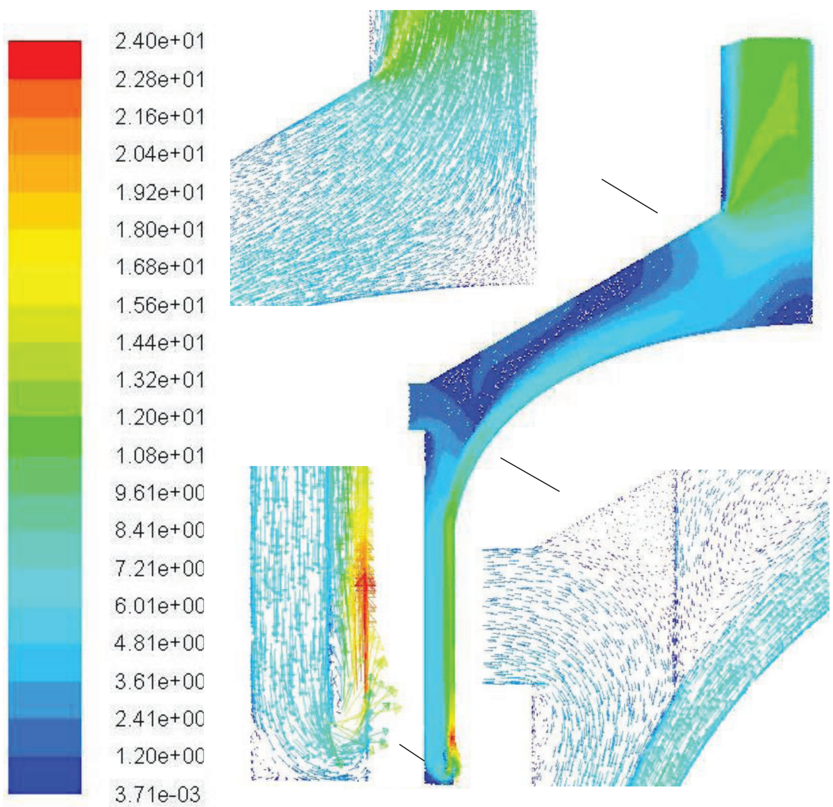

Figure 7. Velocity Vector Field

When the outside surface temperature of steel CV is 148.85 ^{o}C, the mass flow rate of air natural convection calculated here is 69.16 kg/s, the average velocities at the inlet and outlet are 2.059 m/s and 9.562 m/s, respectively. Reynolds numbers calculated based on them are 6.65×10^{5} and 5.24×10^{6} respectively and thus air flow in the annulus is turbulent.

Velocity vectors in vertical midsection of the annulus were shown in Fig. 7. Air natural circulation from the inlet to the outlet was formed in the annulus. Due to the existence of air baffle, air first goes downwards, changes the direction at the bottom of the air baffle, and then flows upwards along the outside surface of steel CV. It slowly turns direction at the upper part of the steel CV and exists from the annulus at the outlet. Since the cross section of the riser section is smaller than that of downcomer, air velocity in the riser section is higher than air velocity in the downcomer. The highest velocity in the riser section is about 24 m/s. From the figure, it can be observed that the velocity field in the riser section is not symmetrical parabolas. The high surface temperature of steel CV makes the local air density smaller and then the upward buoyancy enhances flow locally.

Temperature field of the calculation region was shown in Fig. 8. The temperature of air in the downcomer changes very little in the flow direction due to the existence of air baffle. In the riser section, air temperature increases quickly in the flow direction because of the high surface temperature of steel CV. It can be seen that, in the riser section, the surface temperature of air baffle is higher than air temperature, meaning that the thermal radiation from the steel CV to the air baffle works and heats the air baffle.

For the computational region, i.e., the 30° portion, the total heat transfer rate and radiation heat transfer

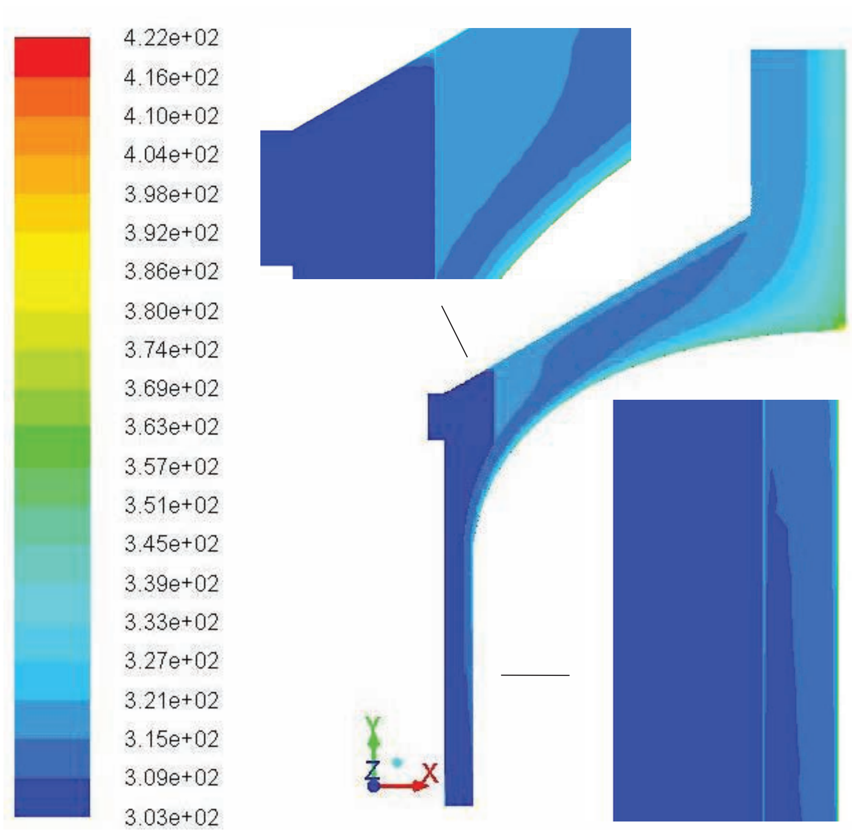

Figure 8. Temperature Contours

rate can be obtained directly from the results report of the ANSYS FLUENT. They are the integration of heat fluxes over the steel CV surface. The natural convection heat transfer rate can be obtained from their subtraction. The total heat removal power of PCS is 12 times the total heat transfer rate of the computational region. From this simulation, the total heat removal power of PCS was 13.55 MW, thermal radiation power 3.383 MW and natural convection power 10.164 MW. The comparison of the results of this work with those of Wang et al. [2] was listed in Table I. We can see that the total heat removal power obtained from this work is also smaller than the decay power (17.48 MW) at the time of 72 hours after break accident. In other words, the PCS can't completely remove all the decay heat from inside containment to the environment just through air natural circulation and thermal radiation. At that time, if without human intervention, the pressure and temperature of inside containment will rise and threaten the integrity of containment. This conclusion is the same with that of Wang et al. [2].

Table I Comparison of Results

Reference	Thermal Radiation Power (MW)	Natural Convection Power (MW)	Total Heat Removal Power (MW)
Wang et al.[2]	4.491	6.599	11.09
This work	3.383	10.164	13.547

Since natural circulation is driven by density difference due to temperature difference, boundary conditions significantly affect the heat transfer performance of PCS. Here influences of the inlet air temperature, the steel CV outside surface temperature, and geometrical size on the heat transfer performance of PCS will be discussed below. Notice that in Figures 9-14 the heat transfer rates shown are only for the 30° portion.

The effects of air inlet temperature were shown in Figures 9 and 10. From Fig. 9, it can be seen that with the increase of air inlet temperature, the heat transfer rate (HTR) of thermal radiation (TR) and that of natural circulation (NC) decrease linearly. The reason for the decrease of NC HTR is obvious. For thermal radiation, with the increase of air inlet temperature, the temperatures of the shielding building inside surface, the air baffle, and the lower plane will increase subsequently and thus its HTR decreases with the increase of air inlet temperature. From the figures, the HTR of NC decreases significantly, however, that of TR almost keeps constant. This means that air inlet temperature affects the heat transfer

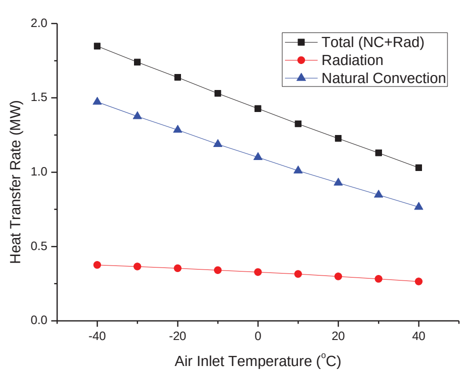

Figure 9. Variation of Heat Transfer Rate with Air Inlet Temperature

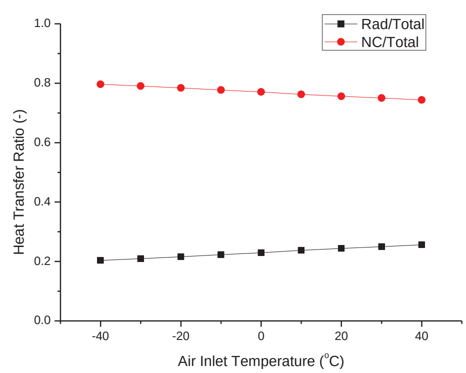

Figure 10. Variation of Heat Transfer Ratio with Air Inlet Temperature

performance of NC more significantly than that of TR. The total HTR (equals to NC part plus TR part) almost follows the tendency of NC HTR. From the Fig. 10, the tendencies of ratios are linear, but the heat transfer ratio of radiation increases with the increase of the inlet air temperature, different with that of NC. This also is due to the bigger effect of air inlet temperature on the heat transfer performance of NC.

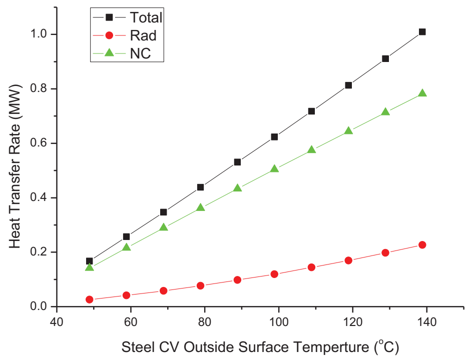

Figure 11. Variation of Heat Transfer Rate with Steel CV Outside Surface Temperature

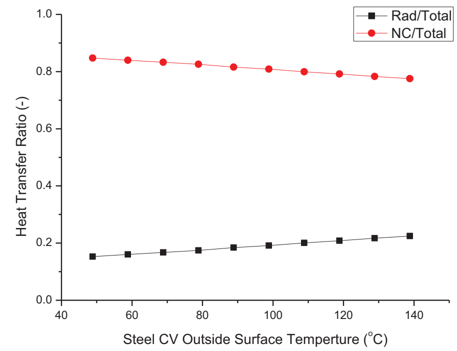

Figure 12. Variation of Heat Transfer Ratio with Steel CV Outside Surface Temperature

The effects of steel CV outside surface temperature were shown in Figures 11 and 12. Values of heat transfer rates and ratios are also listed in Table II. It can be seen that with the increasing of the temperature, the NC HTR increases almost linearly, however, from Table II and Fig. 12 the TR HTR tends to increase with a little bit larger pace, 9 times from 0.0256 to 0.2269 MW for TR HTR. The reason may be that TR HTR is proportional to the fourth power of the surface temperature. The heat transfer ratio of TR increases almost linearly with the steel CV outside surface temperature for a range from about 50 to 140 ℃. There is no minimum value as observed by Wang et al. [2]. They found that the fraction of TR in the PCS heat removal power is smallest when the outside surface temperature of steel containment is about 80 ℃. Table II also showed variations of other parameters. From the table, it can be seen that air flow rate changes little with increasing of the steel CV outside surface temperature.

Table II Variation of Parameters with Steel CV Outside Surface Temperature

Steel CV Outside Surface T. (ºC)	Air at outlet				Heat Transfer Rate			Heat Transfer Ratio	
	Vel. (m/s)	Mass Flowrate (kg/s)	Density (kg/m^3)	T. (ºC)	Rad. (MW)	NC (MW)	Total (MW)	Rad. /Total (-)	NC /Toal (-)
48.85	9.342	69.86	1.144	35.55	0.0256	0.1415	0.1671	0.1530	0.8470
58.85	9.437	69.95	1.134	38.25	0.0411	0.2156	0.2568	0.1602	0.8398
68.85	9.546	70.05	1.123	41.35	0.0580	0.2888	0.3468	0.1673	0.8327
78.85	9.615	70.2	1.117	42.95	0.0765	0.3617	0.4382	0.1746	0.8254
88.85	9.65	70.13	1.113	44.35	0.0978	0.4331	0.5309	0.1841	0.8159
98.85	9.696	70.37	1.111	44.95	0.1192	0.5037	0.6229	0.1913	0.8087
108.85	9.732	70.36	1.107	46.05	0.1440	0.5739	0.7179	0.2006	0.7995
118.85	9.774	70.48	1.104	46.95	0.1690	0.6438	0.8132	0.2083	0.7917
128.85	9.813	70.52	1.1	47.95	0.1977	0.7130	0.9107	0.2171	0.7829
138.85	9.857	70.65	1.096	48.95	0.2269	0.7823	1.0091	0.2248	0.7752

In order to explore the applicability of the PCS in smaller modular reactors, the geometry size influence on the air coolability was investigated as well. Figures 13 and 14 showed the effects of geometric size. The three dimensions, x, y and z, of the computational object were scaled by a factor. It can be seen that with the increasing of the scaling factor, both TR HTR and NC HTR increase smoothly, however, NC HTR in a faster pace. Since NC is governed by the balance between the driving force induced by fluid density difference and pressure loss including friction and form loss, with the increasing of the scaling factor, the height of the annulus and thus the driving force increases, however, the total pressure loss may

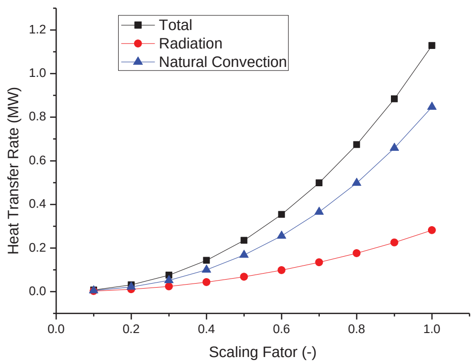

Figure 13. Variation of Heat Transfer Rate with Scaling Factor

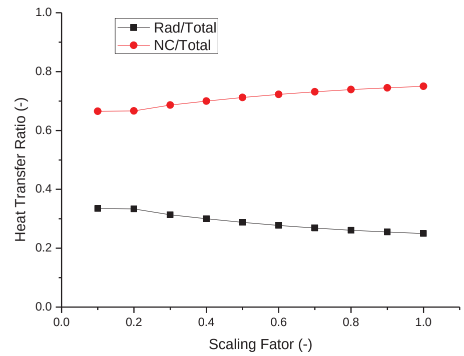

Figure 14. Variation of Heat Transfer Ratio with Scaling Factor

not increase with the height as fast as the driving force since the frictional coefficient decreases with increasing the hydraulic diameter, therefore they reach a new balance at a higher flow rate. This is the reason why NC HTR increases in a faster pace.

6. CONCLUSIONS

Numerical simulation of air natural circulation and thermal radiation was performed to investigate the air coolability of PCS without falling film, the following conclusions may be drawn:

(1) At the time of 72 hours after break accident, if without human intervention, the AP1000 PCS can't completely remove all the decay heat from inside the containment to the environment just through air natural circulation and thermal radiation. The pressure and temperature inside the containment will rise and threaten the integrity of containment.

(2) With the increase of air inlet temperature, the heat transfer rate of thermal radiation and that of natural circulation decrease. Air inlet temperature affects the heat transfer performance of natural circulation significantly, but it affects that of thermal radiation very little.

(3) With the increasing of steel CV outside surface temperature, the heat transfer rate of natural circulation increase, however, the thermal radiation heat transfer rate tends to increase in a faster pace. For the steel CV temperature ranging from about 50 to 140 ℃, no minimum value of the fraction of thermal radiation in the PCS heat removal power was observed in this study. Geometry size affects the heat transfer rate of natural circulation significantly.

ACKNOWLEDGMENTS

This work was performed under the auspices of SNPTC Staff Independent Innovation Fund. The project number is SNP-KJ-CX-2014-17.

REFERENCES

1. C.G Lin, *An Advanced Passive Plant AP1000*, 195-199, Atomic Energy Press, Beijing China (2008).
2. H.Wang, Q. Guo, and Q. Chen. "Numerical research on performance of AP1000 passive containment cooling system without falling film", *Proceedings of the 21st Int. Conf. on Nuclear Engineering*, Chengdu, China, Jul. 29-Aug.2, 2013, ICONE21-15644 (2013).
3. *ANSYS FLUENT Release 14.0,* ANSYS Inc. (2011).
4. A. Frisani, V. M. Ugaz, Y. A. Hassan, "Analysis of RCCS heat exchange for benchmarking of CFD codes", *Proceedings of the 18st Int. Conf. on Nuclear Engineering*, Xi'an, China, May 17-21, 2010, ICONE18-29884 (2010).